

# ROSAT OBSERVATIONS OF THE VELA PULSAR

F.D. Seward<sup>1</sup>, M.A. Alpar<sup>2</sup>, C. Flanagan<sup>3</sup>, U. Kiziloglu<sup>2</sup>, C. Markwardt<sup>4</sup>, P. McCulloch<sup>5</sup>, H. Ogelman<sup>6</sup>

To appear in The Astrophysical Journal

## ABSTRACT

The ROSAT HRI was used to monitor X-ray emission from the Vela Pulsar. Six observations span 2-1/2 years and 3 glitches. The summed data yield a determination of the pulse shape, and X-ray emission from the pulsar is found to be 12% pulsed with one broad and two narrow peaks. One observation occurred 15 days after a large glitch. No change in pulse structure was observed and any change in X-ray luminosity, if present, was less than 3%. Implications for neutron star structure are discussed.

Subject headings: pulsar, neutron stars, X-rays

## 1. INTRODUCTION

The Vela Pulsar, located at the center of a prominent supernova remnant and with characteristic age ( $\tau=2p$ ) of  $1.1 \times 10^4$  years, is "young". The distance to the pulsar is only 500 pc (Frail and Weisberg, 1990) and the column density of absorbing material ( $< 2 \times 10^{20}$  atoms  $\text{cm}^{-2}$  or less) is low. Thus, soft x-rays from the pulsar can be detected and have been interpreted as thermal radiation from the surface of the hot neutron star. (Hamden et al. 1985, Ogelman et al. 1993).

Like the younger Crab Pulsar, the Vela Pulsar is a source of high energy gamma-rays (Kanbach et al. 1994). It is well known that the Crab Pulsar exhibits approximately the same pulse structure at  $\gamma$ -ray, X-ray, and optical wavelengths, two rather narrow pulses, separated by 0.4 in phase. The Vela Pulsar, however, emits a pulse waveform which varies with energy (Grenier et al. 1988). At 100 MeV, there are two narrow pulses with width and spacing almost identical to those from the Crab Pulsar. In visible light, there are two broad pulses separated by only 0.2 in phase. X-ray pulsations from the Vela Pulsar were recently discovered by Ogelman et al. (1993). They found the pulsed fraction to be 10% (in contrast to 100% for the Crab Pulsar) and the pulse structure, complex.

Like other isolated pulsars, the period of the Vela Pulsar, has been observed to increase steadily and regularly with time. There are, however, in the Vela Pulsar, discontinuities or "glitches" in the timing which occur on average every 2.5 years. To observe this phenomenon, the radio signal is monitored daily (McCulloch et al. 1988). During a glitch, the frequency of radio pulsations,  $\nu$ , increases suddenly by 1 part in  $10^6$  and the frequency derivative,  $\dot{\nu}$ , increases by 1 part in  $10^2$  and then recovers steadily

from this transient behavior. Duration of the recovery is 10–100 days.

Glitches offer a rare opportunity to learn something about the interior of the neutron star and much has been learned from radio-timing data alone (Link et al. 1992). It is believed that, during the glitch, rotational energy is dissipated in the stellar interior. The time scale of energy flow depends on the size of the star, the nature of the glitch mechanism, and the structure of the outer layers of the star. The amount of thermal energy generated and conducted to the surface could be enough to cause an observable increase in temperature of the surface (van Riper et al. 1991). We attempted to observe this with ROSAT.

## 2. ROSAT OBSERVATIONS

The requirement that the ROSAT solar panels point at the sun forbids observations of the Vela Pulsar except during the intervals, 22 April to 26 June and 25 October to 26 December. During these intervals, we obtained data with the ROSAT HRI 6 times. There were also two previous ROSAT PSPC observations. Parameters of the observations are listed in Tables 1 and 2, and exposure times range from 20 to 60 ks.. Figure 1 compares the dates of ROSAT observations with times of recent glitches.

The time structure of the ROSAT observations was not ideal for pulsar work. Typically the target was observed for 1000–3000 seconds during each 95-minute orbit but with some long intervals devoted to other targets. A typical data stream for an observation contains 10 hours exposure spread over 15 days time.

<sup>1</sup>SAO, 60 Garden Street, Cambridge, MA 02138

<sup>2</sup>Middle East Technical University, Astrophysics Div., Inonu Blvd., 06531 Ankara, Turkey

<sup>3</sup>Hartebeesthoek Radio Observatory, P.O. Box 443, Krugersdorp, Transvaal 1740, South Africa

<sup>4</sup>NASA/GSFC, Code 662, Greenbelt, MD 20771

<sup>5</sup>University of Tasmania, School of Physics, G.P.O. Box 252-21, Hobart, Tasmania, Australia

<sup>6</sup>University of Wisconsin, Department of Physics, 1150 University Avenue, Madison, WI 53706

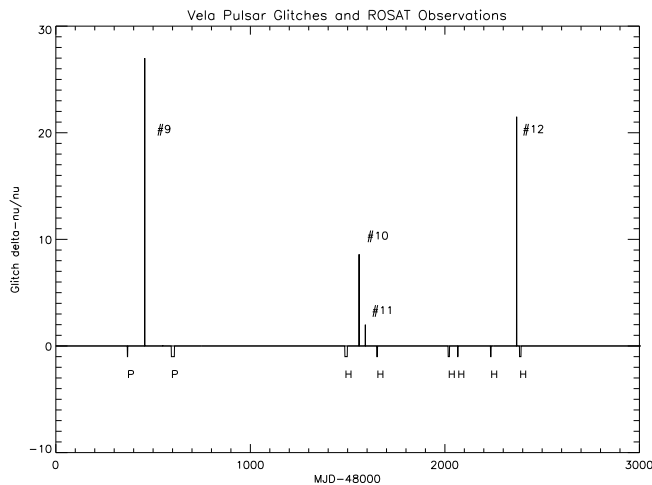


Figure 1: Time history of Vela Pulsar glitches and ROSAT observations. Observations are below the horizontal line. P indicates PSPC, H indicates HRI. Width of the pip shows time spread of data during that observation. Glitches are above the line. Height of the glitch-line is proportional to  $\Delta\nu/\nu$ .

In the longest exposure (60 ks spread over 14 days) the pulsed signal was strong enough so the pulsar frequency could have been identified using x-ray data alone, even without the known radio-measured pulsar frequency. In the shortest exposure, it was necessary to know the approximate radio-measured pulsar frequency to find the x-ray period.

We searched for the most significant x-ray period by epoch folding over a range bracketing the period calculated from a radio period measured within a few days of the ROSAT observation. In every case, the period calculated from the radio ephemeris agreed within a few ns with the most significant x-ray period in that range. The derived X-ray pulse shape, however, is very dependent on the value used for the period. A shift of a few ns makes a difference. We therefore used the Hartbeesthoek and the U.Tasmania radio data to calculate the expected period to 0.1 ns and used this period to fold the x-ray data. Table 1 lists the input radio data and table 2, the pulse periods calculated (and observed) at the start of each ROSAT observation.

We tried to use the radio observations to calculate the absolute phase of x-ray data but got errors of 0.2 in phase. To better determine the structure of the x-ray pulse, we aligned the HRI observation in phase using the highest peak and summed the observations. 40 phase bins were used. If this procedure were followed using random data, we would, of course, get a single, apparently significant, peak in the summed light curve, but there should not be other significant structure. Since the summed Vela Pulsar light curve shows a second sharp peak, we believe this procedure is valid and the observed structure to be real.

Figure 2 shows the light curve generated by adding the 3 longest pre-glitch observations (May 94, Oct 94, June 96). The pulse structure was clear in each of these and the phase alignment was done to an accuracy of .025

in phase. The same shape is apparent in all the longer individual HRI observations and, is similar to that reported by Ogelman et al. (1993) for the 1991 PSPC observations. There are 2, sometimes 3, narrow peaks superimposed on a broader structure. The Oct 95 and Dec 95 light curves were not as good statistically and the structure not as clear. The appearance of shorter observations is sometimes almost a sawtooth with one prominent peak and valley.

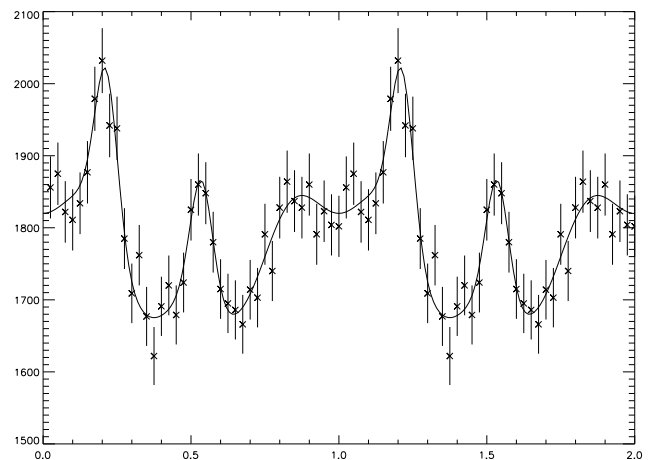


Figure 2: Pre-glitch Vela Pulsar light curve. HRI count rate vs. phase over two complete cycles. The 3 longest pre-glitch HRI observations have been phase-matched using the strongest peak, summed, and fitted with an empirical curve. Errors shown are one sigma. Total observation time was 123 ks.

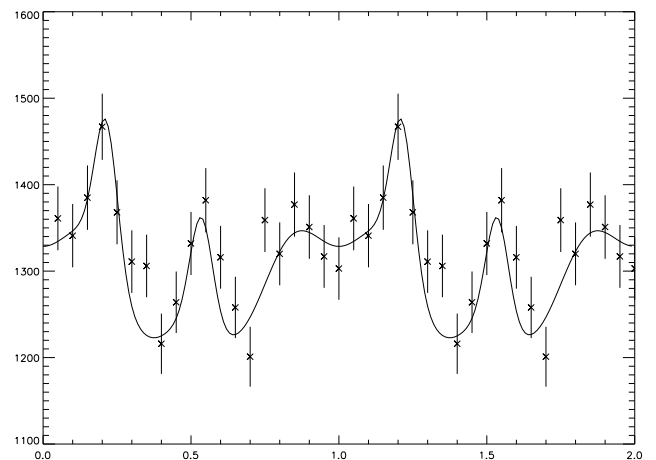


Figure 3: Post-glitch-12 light curve. October 96 data are compared with the pre-glitch empirical fit of Figure 2. Total observation time was 43 ks. This observation started 15 days after glitch 12 and is our best chance, in these data, to observe any post-glitch change in intensity or pulsed waveform. The post-glitch waveform is, within observational limits, the same as the average pre-glitch waveform.

Figure 3 shows the post-glitch October '96 data alone. This observation started 15 days after glitch 12 and is our best chance, in these data, to observe any post-glitch

change in intensity or pulsed waveform. The post-glitch waveform is, within observational limits, the same as the average pre-glitch waveform. The October '94 observation started 59 days after glitch 11 (which was small) and we have included it in the sum of pre-glitch observations.

An independent technique was used to confirm that pulsed emission was present. The Princeton radio ephemeris was used to calculate the pulsar period at the midpoint of each HRI data set. Data were folded at this period and light curves similar to those illustrated were obtained.

### 3. INTERPRETATION OF PULSED SIGNAL

We assume that the pulse has two components: a broad pulse and two narrow peaks. There is also a large non-varying (probably thermal) component.

We used a  $10^{00}$  radius circular region to extract the pulsar data. The pulsar appeared slightly elongated in all observations because the "wobble" in the ROSAT pointing was not completely removed. This circle was large enough to encompass 85% of the events in the ROSAT point spread function. Table 3 lists the observed components of the HRI signal. Uncertainty in the total rate is due to counting statistics. An order of magnitude larger uncertainty in the signal from the pulsar is due to possible error in subtraction of a contribution from the surrounding diffuse nebula. (Hamden et al. 1985)

To compare pre and post-glitch data we made an empirical fit to the data shown in Figure 2. This fit is indicated by the solid line. Because it appears more square than a pure sine wave, the broad pulse form assumed is  $\cos^2$  ( $l=3$ )  $\cos^6$ . The two narrow peaks are assumed to be Gaussian with identical widths. The fit to Figure 2 is  $I = 0.573 + 0.029 [\cos^2$  ( $l=3 \cos^6$ )  $]+ 0.071e^{\frac{(\phi-214)^2}{2(0.38)^2}} + 0.056e^{\frac{(\phi-535)^2}{2(0.38)^2}}$ .  $\phi$  is phase (0-1) and the units of  $I$  are ROSAT HRI counts  $s^{-1}$ . The two narrow peaks have FWHM of 0.09 in phase and are separated by 0.32 in phase. As summarized in table 3, after subtraction of a nebular component, 12% of the pulsar emission is pulsed with 8% in the broad pulse and 4% in the two narrow peaks.

The 1991 PSPC data were re-analyzed using the same techniques as for the HRI data. A  $15^{00}$  radius region was used to extract the pulsar signal and data were again folded at the radio-determined pulsar frequency. The April 1991 PSPC light curve is compatible with the fit to the HRI data. Epoch folding of the December 1991 data produced no clear indication of the pulsar which probably indicates a timing problem in our December 1991 data.

### 4. THE ABSOLUTE RATE

The countrate of the pulsar (and immediate surroundings) was monitored by extracting events from a circle  $15^{00}$  in radius, centered on the pulsar. To minimize the effect of variations in detector efficiency and background, the rate from the surrounding annulus with inner and outer radii of  $15^{00}$  and  $80^{00}$  was also monitored and used for normalization. This annulus contains a relatively bright region

of diffuse emission surrounding the pulsar which should not vary on the time scale of this observation. The central region should contain 87% of the pulsar emission (from the ROSAT point response function in David et al 1998) and is large enough to allow for the observed attitude smearing of a few arcseconds.

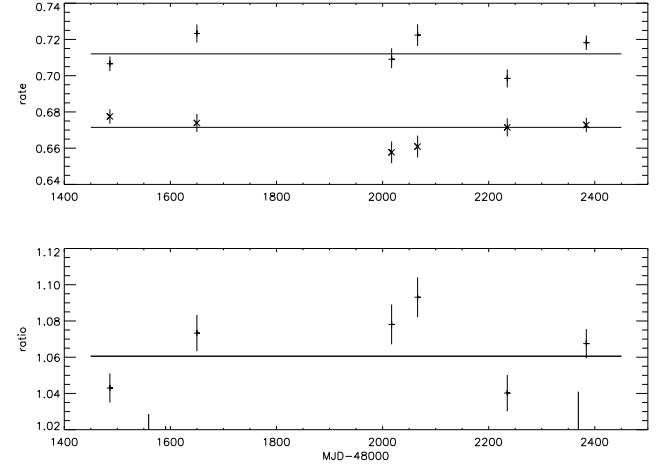


Figure 4: Pulsar brightness vs time. Count rate from the pulsar and immediate surroundings for the 6 HRI observations. Top curve (+) is the rate taken from a small region around the pulsar. Middle curve (X) is from a surrounding annulus and includes diffuse emission only. Bottom curve (+) is the ratio of the two. Horizontal lines are averages weighted by exposure and glitches are indicated as bold vertical lines on the time axis. Error bars show 1 counting statistics

These data are given in table 4 and plotted in Figure 4. Error bars show 1 counting statistics only which are 1%. No significant variation in the pulsar flux is seen, either in the countrate or normalized countrate. We note that there is a 3% increase in rate after both glitches (or rather a 3% decrease in rate before the glitches) and take this as an upper limit to an observed effect. A 3.0% change in the rate shown in Figure 4 requires a 6.4% change in pulsar flux which, if attributed to black body emission, would correspond to a temperature increase of 1.6%. We also note that the accuracy inferred from Figure 4 is pushing the limit of the ROSAT HRI. Periodic calibrations with the supernova remnant N132D give apparent efficiency variations of up to 5% for unknown reasons (David et al. 1998). Our normalized rates should avoid this as well as any efficiency change which might be associated with a detector gain (high voltage step) change on June 21, 1994 (David et al. 1998), between the first and second HRI observations.

### 5. A SIMPLE ANALYSIS

It is natural to assume that the narrow pulses are of non-thermal origin. The non-thermal gamma-ray pulses are both sharp and double and the phase separation of the two X-ray pulses is intermediate between the phase separation of the two optical and that of the two gamma-ray

pulses (Ram anam urthy, 1994).

The broad pulse could also be non-thermal. The young pulsar, B 0540-69 exhibits a single broad pulse at both X-ray and optical wavelengths (Deeter et al., 1999, Gouies et al., 1992, Manchester and Peterson, 1989). The young pulsar, B 1509-58, also shows a single broad peak in the X-ray band with non-thermal spectrum (Kawai et al 1993). So it is interesting that the Vela pulse waveform shows both narrow Crab-like pulses and the broad pulse associated with two other young pulsars. A thermal origin, however, for either broad or narrow Vela-Pulsar pulses is not ruled out by these data.

Assuming the non-varying component to be thermal, we can derive the temperature and luminosity. (We note that the validity of a black-body approximation to the spectrum is untested and that the derived temperature may not be physical. Nevertheless, the result is useful.) Using a distance of 500 pc, a black body spectrum, a neutron star radiation radius of 10 km, and an interstellar column density of  $5 \times 10^{19}$  atom/cm<sup>2</sup>, the PIMMS program was used to calculate the luminosity and surface temperature,  $T$ , from the ROSAT HRI count rate. Results are listed in Table 5. Because the luminosity varies as  $T^4$ , the 20% uncertainty in count rate of the non-varying component, if thermal, corresponds to a 5% uncertainty in temperature. A more realistic range for parameters can be derived by using extremes of the generally accepted ranges for distance (400-500 pc), neutron star radius (7-15 km), and interstellar column ( $N_H = 0.2 \times 10^{20}$ ). Possible values for  $T$  lie in the range  $5 \times 10^5$  K with corresponding bolometric luminosities of  $2 \times 10^{32}$  erg/s. The most likely fit to our data yields a neutron star temperature of  $8.5 \times 10^5$  K and bolometric luminosity of  $4 \times 10^{32}$  erg/s.

#### 6. APPLICATION TO GLITCH PHYSICS

This null result can limit some values of parameters which describe neutron star structure. The parameters are largely unknown, are not independent, and can be linked through models. Theoretical models start with a model neutron star (a choice of mass and equation of state EOS). The remaining parameters include the initial (preglitch) temperature distribution, the amount of energy  $E$  dissipated in the glitch and the location, or density, where the energy dissipation takes place. This heat, released promptly during the glitch, will diffuse out to the neutron star surface and inward, into the neutron star core. To calculate the postglitch thermal signal on the neutron star surface, models of the heat capacity and thermal conductivity, as well as neutrino emissivities from the interior are required. At the age of the Vela pulsar, the interior of the neutron star is expected to be isothermal with a core temperature extending through the inner crust. The associated surface temperature is determined by conductivities in the outer crust (Gudmundsson, Pethick and Epstein 1981). Calculations of the expected postglitch thermal signal on the surface have been reported by Eichler and Cheng (1989), van Riper, Epstein and Miller (1991), by Chong and Cheng (1994) and by Hirano et al (1996) for various combinations of the parameters. The results are qualitatively similar. All calculations are quite sensitive to the initial value of the surface temperature.

The fractional change in temperature is higher for lower initial temperatures. For a conservative evaluation of our null results, in terms of which model parameters can be ruled out, we take the initial surface temperature to be the highest value, covered in the model calculations,  $10^6$  K. This is also the appropriate choice of initial surface temperature for the Vela pulsar. The ROSAT measurements of Ogelman, Finley and Zimmerman (1993) yield surface temperatures of  $1.5\text{--}1.6 \times 10^6$  K from black body fits to the point source and to the pulsed signal. The model-dependent analysis of the previous section yields a temperature of  $0.85 \times 10^6$  K. The actual value of the surface temperature may be somewhat different but of the same order when neutron star atmosphere models are used.

Van Riper et al (1991) present their results in terms of  $t_{\text{peak}}$ , the time at which the glitch-induced temperature signal on the surface is maximum; the width  $\Delta t$  of this signal and the maximum fractional change in the surface temperature. Contours of  $t_{\text{peak}}$  and  $\Delta t$  for which the postglitch temperature enhancement signal would fall within the range of our observations, 15-22 days after the glitch, correspond roughly to neutron star radii  $R < 13$  Km. Thus for  $T_{s,0} = 10^6$  K our upper limits test the models only for stars with  $R < 13$  Km. The radius of a typical  $1.4 M_\odot$  neutron star is 13.7 Km in the soft Baym, Pethick and Sutherland (1971) equation of state and 13.7 Km for the medium equation of state of Friedman and Pandharipande (1981). For a stiffer equation of state like the Pandharipande, Pines and Smith (1976) model the radius of a  $1.4 M_\odot$  star is 18.6 Km, so our results do not test the models if the neutron star EOS is actually stiffer. If the energy release  $E$  in the glitch was  $10^{42}$  ergs, the thermal signal would violate our upper bound if the glitch dissipated energy at densities  $> 10^{13}$  gm/cm<sup>3</sup> or less so it is likely that  $E < 10^{42}$  ergs, conditional on the values.  $E = 10^{43}$  ergs can be ruled out altogether, for no matter at what the glitch energy was dissipated, the signal on the surface would violate our upper bounds.

Chong and Cheng (1994) plot their results for  $1.4 M_\odot$  neutron stars of different EOS, initial surface temperatures and  $E$ , taking the density at which the glitch energy is dissipated to be  $\rho = 10^{13}$  gm/cm<sup>3</sup> for all cases. Taking their model for a soft BPS star with the core temperature  $T_c = 10^8$  K, corresponding to an initial surface temperature of  $1.27 \times 10^6$  K we find that  $E = 10^{43}$  ergs is ruled out by our results. For the moderately stiff UT equation of state (Wiringa & Fiks 1988) with  $T_c = 10^8$  K and  $T_{s,0} = 10^6$  K, the model prediction for the temperature enhancement at the times of our observations lie below the upper limits, so even  $E = 10^{43}$  ergs is not ruled out. For the stiff PPS star model, with  $T_c = 10^8$  K and  $T_{s,0} = 8 \times 10^5$  K,  $E = 10^{43}$  ergs is ruled out by our upper limits.

Hirano et al (1997) present similar results by marking in the  $A_T = T_s/T_{s,0}$  vs  $t_{\text{peak}}$  plane the maximum  $A_T$  points for different  $1.4 M_\odot$  neutron star models and different densities of energy release. Results are given for various values of the initial surface temperature  $T_{s,0}$  and energy release  $E$ . To check if the predicted signals extend

into our range of observation times, we utilized the temperature evolution for one-dimensional heat conduction, Eq.(4) of Hirano et al. which they quote as representative of the temperature evolution in their detailed numerical results. At  $T_{s,0} = 10^6$  K,  $E = 10^{43}$  ergs is ruled out if the EOS is soft (the Baym, Pethick, Sutherland (1971) model). For a moderately stiff FP star, our results rule out  $E = 10^{43}$  ergs if the energy was released at  $< 3 \times 10^{13}$  gm cm<sup>-3</sup>.

In addition to these model calculations, all of which assume that the glitch induced energy dissipation takes place in a spherically symmetric shell, a recent paper by Cheng, Li and Suen (1998) presents model calculations of the non-spherically symmetric case. These authors calculate the thermal signal on the neutron star surface for the case of glitch induced energy dissipation at densities  $3 \times 10^{12}$  gm cm<sup>-3</sup>  $< < 3 \times 10^{13}$  gm cm<sup>-3</sup>, and within a  $2 \text{ deg} \times 2 \text{ deg}$  solid angle. For  $E = 10^{42}$  ergs a hot spot is found to emerge on the surface, keeping to the same solid angle range and peaking at 274 days after the glitch. During our observations, 15-22 days after the glitch, a 50 percent enhancement in temperature is predicted in the hot spot. The contribution to the total luminosity of this hot spot remains well below our upper limits. The absence of significant changes in the pulse shape of the Vela pulsar before and after a glitch does not lead to a test of the models. The hot spot is at the same angular position as the region of energy dissipation in the glitch. For many values of the angles from the rotation axis and from our line of sight, there would be no modulation in the observed signal. Furthermore, the energy dissipation might take place in an equatorial belt around the rotation axis, as is likely if the glitch is due to vortex line unpinning (a rotational instability in the neutron star crust superfluid).

Returning to the spherically symmetric models we note that the differences between the model predictions are not important for purposes of comparison with our current upper limits. (These differences are likely to be due to different surface layer compositions in the models in terms of the A and Z of the equilibrium nuclear species, affecting the thermal conductivities (Hirano et al 1997)). Within the uncertainties indicated by these differences, and the large number of unknown parameters, we conclude that our upper bounds on a thermal signal rule out glitches with energy release,  $E$ , greater than  $10^{43}$  ergs.

For superfluid unpinning models of the glitches the energy dissipated is given by:

$$E = I_p \Delta \dot{\Omega} = I \Delta \dot{\Omega} : \quad (1)$$

In these models the glitch reflects a transfer of angular momentum,  $J = I_p \Delta \dot{\Omega} = I \Delta \dot{\Omega}$ , from a component of the neutron star, taken to be the pinned superfluid in the inner crust, to the rest of the star including the observed crust.  $I_p$  is the moment of inertia of the pinned superfluid and  $\Delta \dot{\Omega}$  the decrease in its rotation rate during the glitch.  $I$  is the moment of inertia of the observed crust and most of the neutron star, which is coupled rigidly to the crust.  $\Delta \dot{\Omega}$  is the observed jump in rotation frequency of the crust and  $\Delta \dot{\Omega}$  is the difference in rotation rate be-

tween the superfluid and the normal crust.  $\Delta \dot{\Omega}$  is related to the pinning forces. Our upper bound on  $E$  implies a very loose upper bound  $\Delta \dot{\Omega} < 100 \text{ rad s}^{-1}$ . Recent theoretical work (Pizzochero, Viverit & Broglia 1997) gives pinning energies which imply  $\Delta \dot{\Omega} < 1 \text{ rad s}^{-1}$ . The coupling between the pinned superfluid and the observed crust of the neutron star also entails a continuous rate of energy dissipation, realized through the thermal creep of vortices. In parallel to the glitch associated energy dissipation, this continuous rate is easily shown to be (Alpar et al 1984):

$$E_{\text{diss}} = I_p \dot{\Omega} \Delta \dot{\Omega} : \quad (2)$$

This should supply the thermal luminosity of an old pulsar. Observational upper bounds from the thermal luminosities of older pulsars (Alpar et al 1987, Yancopoulos, Hamilton & Helfand 1994) yield  $\Delta \dot{\Omega} < 1 \text{ rad s}^{-1}$ .

While crustquake models fail to explain the magnitude and rate of glitches of the Vela pulsar, crustquakes may trigger the vortex unpinning and angular momentum transfer that show up as glitches. The crust cracking that triggers a glitch (Ruderman 1991) entails an energy dissipation

$$E = \frac{1}{2} \epsilon \quad (3)$$

where  $\epsilon$  denotes the elastic energy modulus and  $\epsilon$  is the critical strain angle for the breaking of the lattice. For a volume of linear dimensions  $10^5 \text{ cm}$   $= 10^{44}$  ergs. Our upper limit of  $E = 10^{43}$  ergs then implies that  $\epsilon < 10^{-1} \text{ rad s}^{-1}$ . While terrestrial solids have  $\epsilon < 10^{-4}$  or less, there have been speculations that the neutron star crust will have  $\epsilon > 10^{-2}$ , a much larger strength resulting from its unscreened Coulomb interactions. Thus, observations that are sensitive to implied glitch energy dissipation rates  $E = 10^{41}$  ergs will be critical for the crust-breaking models of glitches as well as for the superfluid-unpinning model.

While the present upper limit does not give any stringent constraints on the glitch related energy release, a future detection could yield important clues into the neutron star EOS, since in all calculations, different EOS yield different timescales for the postglitch thermal signal. Post-glitch RXTE-PCA observations of the Vela pulsar, at one, four and nine days, and at about three months following the October 1996 glitch do not constrain models of glitch related energy dissipation (Gurkan et al. 1999). New instruments should have the capability to detect temperature rises from the Vela pulsar at the corresponding levels of sensitivity. The Chandra HRC detector is 3.4 times as sensitive as the ROSAT HRI and can thus collect data equivalent to that shown in Figure 2 in 36 ks. Two such observations, one day and one week after a glitch, should measure an increase in surface luminosity if the energy release is  $10^{41}$  ergs or greater. This time frame does not cover all of parameter space but is probably the best place to search.

This work was supported by NASA through contract NAS8-39073 and grant NAG 5-6853.

## REFERENCES

- Alpar, M. A., Anderson, P. W., Pines, D. & Shaham, J., 1984, *ApJ*, 276, 325.
- Alpar, M. A., Brinkmann, W., Kiziloglu, U., Ogelman, H. & Pines, D., 1987, *A & A*, 177, 101.
- Baym, G., Pethick, C., Sutherland, P., 1971, *ApJ*, 170, 299.
- Cheng, K. S., Li, Y., Suen, W. M., 1998, *ApJ*, 499, L45.
- Chong, N., Cheng, K. S., 1994, *ApJ*, 425, 210.
- David, L. P. et al. 1998, The ROSAT HRI Calibration Report, [http://hea-www.harvard.edu/rosat/rsdc/www/HRI/CAL\\_REPORT/hri.html](http://hea-www.harvard.edu/rosat/rsdc/www/HRI/CAL_REPORT/hri.html).
- Deeter, J. E., Nagase, F., Boynton, P. E., 1999, *ApJ* 512, 300.
- Eichler, D., Cheng, A. F., 1989, *ApJ*, 336, 360.
- Frail, D. A. and Weisberg, J. M., 1990, *AJ*, 100, 743.
- Friedman, B., Pandharipande, V. R., *Nucl Phys A*, 1981, 361, 502.
- Gouies, C., Finley, J. P. and Ogelman, H., 1992, *ApJ* 394, 581.
- Grenier, I. A., Hemmen, W., Clear, J., 1988, *A & A*, 204, 117.
- Gudmundsson, E. H., Pethick, C., Epstein, R. I., 1983, *ApJ*, 272, 286.
- Gurkan, M. A., Baykal, A., Ogelman, H., Alpar, M. A. and Strohmayer, T., 1999, (to be submitted to *A & A*).
- Hamden, F. R., Jr., Grant, P. D., Seward, F. D., Kahn, S. M., 1985, *ApJ*, 299, 828.
- Hirano, S., Shibasaki, N., Umeda, H., Nomoto, K., 1997, *ApJ*, 491, 286.
- Kanbach, G., et al. 1994, *A & A* 289, 855.
- Kawai, K., Okayasu, R., Sekimoto, Y., 1993, *AIP Conference Proceedings* 280, 213.
- Link, B., Epstein, R. I., Van Riper, K. A., 1992, *Nature* 359, 616.
- Manchester, R., N., Peterson, B., A., 1989, *ApJ* 342 L23.
- McCulloch, P. M., Hamilton, P. A., McConnell, D., King, E. A., 1990, *Nature*, 346, 822.
- Ogelman, H., Finley, J. P., Zimmermann, H. J., 1993, *Nature*, 361, 136.
- Pandharipande, V. R., Pines, D., Smith, R. A., 1976, *ApJ*, 208, 550.
- Pizzochero, P. M., Viverit, L. & Broglia, R. A., 1997, *Phys. Rev. Lett.*, 79, 3347.
- Ramamoorthy, P. V., 1994, *A & A* 284, L13.
- Ruderman, M. A., 1991, *ApJ*, 366, 261.
- Van Riper, K. A., Epstein, R. I., Miller, G. S., 1991, *ApJ*, 381, L47.
- Wiringa, R. B., & Fiks, V., 1988, *Phys. Rev. C*, 38, 1010.
- Yanopoulos, S., Hamilton, T. T. & Helfand, D. J., 1994, *ApJ*, 429, 832.

| Table 1          |                               |   |                  |  |
|------------------|-------------------------------|---|------------------|--|
| Date<br>(UT)     | Rotation<br>Frequency<br>(Hz) | Frequency<br>Derivative<br>$10^{12} \text{ (Hz s}^{-1}\text{)}$ | Epoch<br>(MJD)   |  |
| 14-26 May 94     | 11.197 366 280 36             | -15.5881  | 49492.274659780  |  |
| 25-28 Oct 94     | 11.197 160 398 75             | -15.6554  | 49653.5062011504 |  |
| 27 Oct -2 Nov 95 | 11.196 668 608 990            | -15.5921  | 50017.020877910  |  |
| 15-16 Dec 95     | 11.196 603 154 274            | -15.5858  | 50066.015970352  |  |
| 1-3 Jun 96       | 11.196 376 285 216            | -15.5777  | 50236.139720991  |  |
| 28 Oct -4 Nov 96 | 11.196 198 755 884            | -15.5693  | 50385.205072337  |  |

| Table 2          |            |                              |                        |   |                 |
|------------------|------------|------------------------------|------------------------|---|-----------------|
| Date<br>(UT)     | Instrument | Exposure<br>Live time<br>(s) | X-ray<br>Period<br>(s) | Period<br>Derivative<br>$10^{13} \text{ (s s}^{-1}\text{)}$ | Epoch<br>(MJD)  |
| 14-26 May 94     | HRI        | 62090                        | 0.089 306 649 49       | 1.2433  | 49486.169164815 |
| 25-28 Oct 94     | HRI        | 31545                        | 0.089 308 327 69       | 1.2486  | 49650.775217647 |
| 27 Oct -2 Nov 95 | HRI        | 19409                        | 0.089 312 279 83       | 1.2437  | 50017.896366423 |
| 15-16 Dec 95     | HRI        | 20380                        | 0.089 312 801 95       | 1.2432  | 50066.494671817 |
| 1-3 Jun 96       | HRI        | 28834                        | 0.089 314 611 67       | 1.2427  | 50235.015672685 |
| 28 Oct -4 Nov 96 | HRI        | 43194                        | 0.089 316 027 86       | 1.2520  | 50384.625402581 |

| Table 3  |        |       |
|--|--------|-------|
| Total rate within $10^0$ radius circle ( $\text{s}^{-1}$ ) | 0.585  | .005  |
| non X-ray and diffuse background                           | 0.0007 | .0001 |
| contribution from surrounding nebula                       | 0.258  | .066  |
| total signal from Vela PSR                                 | 0.326  | .066  |
| 2 narrow pulses  | 0.0122 | .003  |
| broad-pulse  | 0.0277 | .007  |
| steady (thermal?)  | 0.286  | .066  |

| Table 4 |              |                 |      |
|---------|--------------|-----------------|------|
| Date    | Average Rate | Normalized Rate |      |
| May 94  | 0.707 .004   | 1.043           | .008 |
| Oct 94  | 0.723 .005   | 1.073           | .010 |
| Oct 95  | 0.709 .006   | 1.078           | .011 |
| Dec 95  | 0.722 .006   | 1.093           | .011 |
| Jun 96  | 0.699 .005   | 1.040           | .010 |
| Oct 96  | 0.718 .004   | 1.067           | .008 |

| Table 5          |   |                |             |                           |   |
|------------------|---|----------------|-------------|---------------------------|---|
| Distance<br>(pc) | ISM                                     | Neutron Star   |             | T<br>( $10^5 \text{ K}$ ) | $L_{\text{bol}}$<br>( $10^{32} \text{ erg/s}$ ) |
|                  | Column<br>( $10^{20} \text{ cm}^{-2}$ ) | Radius<br>(km) | kT<br>(keV) |                           |   |
| 500              | 0.5                                     | 7              | .082        | 9.5                       | 3.7   |
| 500              | 0.5                                     | 10             | .070        | 8.5                       | 3.8   |
| 500              | 0.5                                     | 15             | .055        | 6.4                       | 4.1   |
| 500              | 0.2                                     | 10             | .066        | 7.7                       | 3.0   |
| 500              | 2                                       | 10             | .082        | 9.5                       | 7.0   |
| extremes         |   |                |             |                           |   |
| 500              | 2                                       | 7              | .095        | 11                        | 8.2   |
| 400              | 0.2                                     | 15             | .047        | 5.5                       | 1.9   |